CrossMark

ARTICLE

Enhanced electrocatalytic hydrogen evolution activity of nickel foam by low-temperature-oxidation

Binhong He
College of Chemistry and Chemical Engineering, Hunan University, Changsha 410012, People's Republic of China; and School of Chemistry and Chemical Engineering, Hunan Institute of Science and Technology, Yueyang 414006, People's Republic of China

Yafei Kuang[a)]
College of Chemistry and Chemical Engineering, Hunan University, Changsha 410012, People's Republic of China

Zhaohui Hou and Minjie Zhou[b)]
School of Chemistry and Chemical Engineering, Hunan Institute of Science and Technology, Yueyang 414006, People's Republic of China

Xiaobo Chen[c),d)]
Department of Chemistry, University of Missouri—Kansas City, Kansas City, Missouri 64110, USA

(Received 8 September 2017; accepted 13 November 2017)

Designing advanced nonprecious metal electrocatalysts to reduce overpotential and accelerate hydrogen evolution reaction (HER) has attracted considerable attention. However, improving the sluggish kinetics for electrocatalytic HER in alkaline media is still a great challenge. Herein, we found that amorphous NiO nanoclusters directly grown on nickel foam (NiO/NF) as a bifunctional HER catalyst demonstrated an ultrahigh electrocatalytic activity in alkaline environment. Such excellent HER performance of NiO/NF might mainly originate from the exposed interfaces of metallic Ni and amorphous NiO. The coordinatively unsaturated amorphous NiO domain is propitious to the adsorption of water molecule and the successive cleavage of HO–H bond, while the neighboring metallic Ni domain is beneficial to the adsorption of resulting H_{ads} intermediate and recombination into hydrogen molecules, thus expediting the HER toward lower overpotential. These findings may open a window to the design and preparation of earth-abundant, low-cost metal oxide/metal electrocatalysts with desirable HER activities.

I. INTRODUCTION

The significant concerns of rapid fossil fuel consumption and carbon dioxide increase in the environment have been driving the development of renewable energies and technologies,[1] among which the electrochemical water splitting for the hydrogen production is regarded as one of the most important approaches for clean and scalable energy substitutes due to its low energy consumption, short reaction period, high-purity product, and environmentally friendly process.[2] The electrocatalytic splitting process of water contains two half-reactions: the hydrogen evolution reaction (HER) and the oxygen evolution reaction (OER) with the following equations $2H^+ + 2e^- \rightarrow H_2$ and $2H_2O \rightarrow 4e + 4H^+ + O_2$, separately. Assuming that the electrochemical reaction is ideal and the Faradic efficiency is 100%, the volume of produced oxygen is half as much as the evolution volume of hydrogen, and the total amount of such two gases is in direct proportion to the quantity of the electrical charge provided for the electrolytic reaction. To improve the electrolysis efficiency, seeking a highly active electrocatalyst for the HER at a low overpotential is indispensable. Precious metals, such as platinum (Pt), have been regarded as one of the state-of-the-art catalysts for HER in acidic medium due to their small hydrogen adsorption free energy (approximately zero), while high cost and scarcity seriously hinder their widespread application on the large-scale generation of hydrogen.[3–5] It is thus urgent to develop novel HER catalysts with high efficiency, earth-abundance, and low manufacturing cost.

So far, tremendous efforts have been devoted to the development of nonprecious metal catalysts with high activity for HER.[6–14] Among such materials, Ni-based electrocatalysts have attracted increasing attention owing to their highly catalytic activity for HER and sufficient corrosion resistance in alkaline solutions.[15] Nonetheless, due to the restriction of sluggish kinetics of the Volmer-

Contributing Editor: Edward M. Sabolsky
Address all correspondence to these authors.
[a)]e-mail: yafeik@163.com
[b)]e-mail: zmj0104@126.com
[c)]e-mail: chenxiaobo@umkc.edu
[d)]This author was an editor of this journal during the review and decision stage. For the *JMR* policy on review and publication of manuscripts authored by editors, please refer to http://www.mrs.org/editor-manuscripts/.
DOI: 10.1557/jmr.2017.446

 © Materials Research Society 2017

https://doi.org/10.1557/jmr.2017.446 Published online by Cambridge University Press

step of HER in alkaline solutions, the Ni-based electrocatalysts generally have suboptimal performance, including poor Tafel slopes, a high overpotential, and large energy consumption. To improve the intrinsic catalytic activity, binary or ternary catalytic systems have been obtained such as Ni–Mo,[15,16] Ni–Fe,[17] and Ni–Mo–Zn,[18] etc. According to the Brewer intermetallic bonding theory,[19] when metals with empty or less-filled *d*-orbitals are alloyed with metals with more filled d-bands, a maximum in bond strength and stability of the intermetallic alloy phases is expected, and there is a well-pronounced synergism in electrocatalysis. This synergistic effect often exceeds the effects of the individual parent metals.[20] Mckone and his group reported the synthesis of unsupported Ni–Mo nanopowders and developed it as an excellent catalyst for HER under aqueous acidic and alkaline conditions. The tested results showed that an overpotential of 70 mV was required to drive the current density of 20 mA/cm^2 in alkaline solution, and the overpotential of 80 mV was required to drive the current density of 20 mA/cm^2 in acidic solution.[15] Kardas and co-workers found that the presence of nickel with Fe^{2+} ion increased the electrocatalytic activity of the coating for the HER in 1 M KOH solution when compared to nickel and iron coatings and that the HER activity of the coatings depended on the chemical composition of the composite coatings.[17] Wang et al. found that the addition of Zn in the Ni–Mo–Zn alloy resulted in a rapid increase in the density of states of the Ni 3*d* orbitals at the Fermi level, which consequently resulted in a higher activity for HER.[18] In addition, Ni-based compounds have also exhibited excellent HER activities such as nickel sulfides[21] and nickel phosphides.[22] Feng and co-workers proposed the preparation of Ni_3S_2 nanosheet arrays on nickel foam (NF) as a highly efficient 3D bifunctional electrocatalyst for both the HER and OER. The excellent catalytic activity of the electrocatalyst was mainly due to the synergistic catalytic effects between Ni_3S_2 nanosheet arrays and exposed high-index facets.[21] Lv group found that Ni_3S_2/rGO nanotube arrays directly grown on NF by a facile hydrothermal method exhibited excellent HER activities in alkaline media. The introduction of reduced graphene oxide was expected not only to control the aggregation and the growth of Ni_3S_2 nanosheets but also to increase the number of active sites, improve the conductivity of the composites, and facilitate electron transfer, which was very important for high HER performance.[23] Ma et al. reported nickel phosphide (Ni_xP_y) catalysts with controllable phases as the efficient bifunctional catalysts for water electrolysis. The Ni_xP_y catalysts with the richest Ni_5P_4 phase delivered efficient and robust catalytic performance for HER in the electrolytes with a wide pH range.[24] Based on the current reports on the Ni-based electrocatalyst developments during the past few decades, these catalysts toward HER still face several challenging problems. (i) The catalytic performance of the most reported HER electrocatalysts is much lower than the Pt/C catalyst and need to be further promoted. (ii) These catalysts are usually studied in a strong acidic electrolyte and some of them require toxic gas treatment at elevated temperature. (iii) The hybrid catalysts with a combination of two or more phases cannot easily maintain the HER catalytic activities due to their complicated components and structures. (iv) Most of these electrocatalysts suffer from bad stability and durability toward HER during the electrochemical reaction processes.

Although many HER Ni-based electrocatalysts have exhibited high activities in acid solutions approaching Pt, most of them cannot operate satisfactorily in alkaline electrolytes. Alkaline HER electrocatalysts are more significant for industrial water-alkali and chlor-alkali electrolyzers. Especially, most Ni-based electrocatalysts still cannot achieve enough low HER overpotentials and Tafel slopes in alkaline electrolytes. Previous research studies have demonstrated that the HER activity of Ni metal can be significantly enhanced by surface modification by NiO in alkaline electrolytes.[25–28] At the interfaces of metal Ni and NiO, it is proposed that the metal Ni domain serves as a tank for the H_{ads} intermediate and the NiO domain serves as a tank for OH_{ads} derived from adsorbed water dissociation, thus accelerating HER.[25] Wang and co-workers proposed the preparation of NiO_x@bamboo-like carbon nanotube hybrids for HER. The hybrids exhibited superb catalytic ability and considerable durability in alkaline solution due to the inherent high Ni^0 ratio and Ni^0 on the interface of Ni/NiO hybrids. In addition, they also found that Ni^0 on the interface of Ni/NiO hybrids performed superior activity for water splitting compared with that of bulk Ni^0.[26] Dai and his group reported nanoscale nickel oxide/nickel heterostructures formed on carbon nanotube sidewalls as highly effective electrocatalysts for HER similar to commercial Pt/C.[27] Our group reported that novel crystalline/amorphous core/shell Ni/NiO nanosheets synthesized by hydrogenation treatment of nickel oxide precursors exhibited a high HER activity. Due to the core/shell Ni/NiO nanostructure, the microstructure offered a lot of heterostructural interfaces facilitating adsorbed water dissociation, a lower overpotential (145 mV), and a smaller Tafel slope (43 mV/dec).[28] Furthermore, the similar HER performance for other nonprecious metals were reported by our group.[29–33] In addition, the defect-rich amorphous NiO_x exhibited enhanced HER activities, benefiting from the edges of the nanosized NiO_x clusters which can lower the energy required to dissociate water into H and OH^- and promote the cleavage of the HO–H bond.[34,35] To control the coverage and structure of modified oxide species elaborately, the complicated deposition methods and assisted

https://doi.org/10.1557/jmr.2017.446 Published online by Cambridge University Press

reduction manners must be used; thus, they are still difficult for the practical application.[36] In contrast, an amorphous Ni/NiO nanostructure may be an optimal structure for the water-alkaline HER because it afforded a large Ni/NiO interfacial area and excellent bubble management, as well as long-term stability.[37,38] But it is a challenge to prepare such an amorphous nanostructure through a facile method.

A novel and facile low-temperature-oxidation method had been developed to synthesize amorphous NiO nanoclusters directly grown on NF (3D NiO/NF) in this work. Herein, NF was used as both the Ni source and the substrate/current collector utilizing potassium persulfate (KPS) aqueous solution as the oxidant. The schematic for the water splitting on the 3D NiO/NF interfaces was displayed in Scheme 1. The aims of this design are listed as follows: (i) the uniformly distributed Ni nanoparticles with the neighboring NiO species can exert good synergetic effects to efficiently convert water molecules to H_2 and (ii) the amorphous NiO nanoclusters are in good contact with the current collector, which is very beneficial to the charge transfer and mass transport due to inward diffusion of the electrolyte and outward diffusion of gas bubbles. Meantime, the close contact between active species endues the catalyst excellent long-term stability. The experimental results showed that the as-obtained sample possessed an extremely high HER activity in alkaline media. The onset potential of the 3D NiO/NF composite electrode was close to 0 V versus RHE, and only a small overpotential of ~70 mV was needed to drive a current density of 10 mA/cm^2 with a Tafel slope of 65 mV/dec. In addition, the as-obtained 3D NiO/NF composite electrode was characterized by X-ray diffraction (XRD), field-emission scanning electron microscopy (FESEM), transmission electron microscopy (TEM), high-resolution transmission electron microscopy (HRTEM), and X-ray photoelectron spectroscopy (XPS). Moreover, the electrochemical performance of the as-synthesized electrode was estimated by means of pseudo-steady-state polarization curves and electrochemical impedance spectroscopy (EIS) in 1.0 M KOH solution.

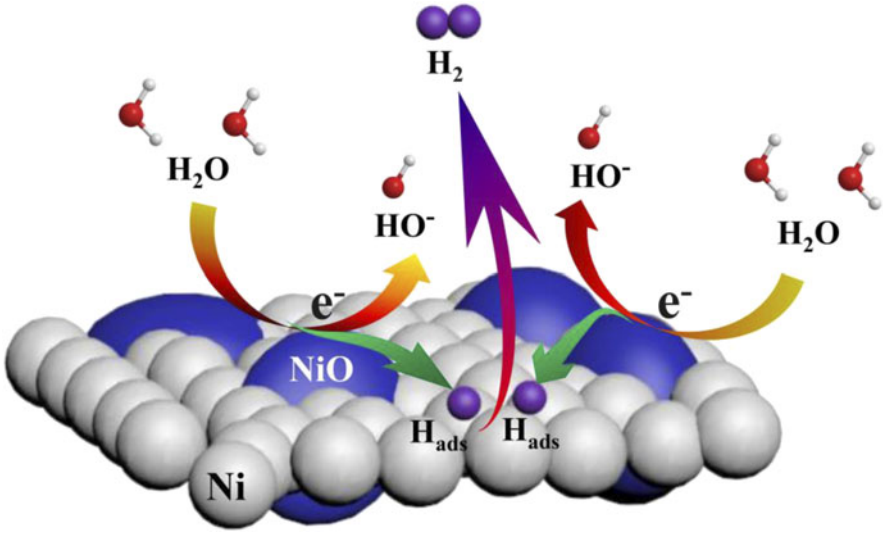
II. EXPERIMENTAL SECTION

A. Materials

NF (300 × 200 × 1.6110 PPI, 320 g/m^2) was purchased from Changsha Lyrun Material Co., Ltd., Changsha, China. Potassium persulfate ($K_2S_2O_8$), concentrated hydrochloric acid (HCl, 37 wt%), potassium hydroxide (KOH), phosphate buffered solution, and acetone (CH_3COCH_3) were obtained from Sinopharm Chemical Co., Ltd., Beijing, China. Commercial Pt/C (20 wt% Pt/XC-72) and Nafion (5 wt%) were purchased from Sigma-Aldrich, Shanghai, China. Deionized (DI) water was prepared by the Millipore Milli-Q water purification system (18.2 MΩ), Millipore, Molsheim, France. All reagents were used as-received.

B. Synthesis of NiO/NF composite

NF (1 × 1 cm) was pretreated with acetone, 3 M HCl, and DI water for 10 min under ultrasonication, respectively. In a typical synthesis, 2.03 g of potassium persulfate (7.5 mmol) was dissolved in 50 mL of DI water in a glass bottle with vigorous stirring for 30 min until a transparent solution (0.15 M) was obtained. A piece of the pretreated NF was then immersed into the above solution, and the reaction was maintained for 6 h at room temperature. After the reaction, NF was taken out, washed with DI water repeatedly, and dried overnight in



SCHEME 1. Schematic for HER on 3D NiO/NF interfaces. Herein, water is reduced on NiO sites and the formed H_{ads} intermediates spillover to nearby Ni sites. Subsequently, two H_{ads} intermediates recombine to H_2.

https://doi.org/10.1557/jmr.2017.446 Published online by Cambridge University Press

a vacuum oven at 60 °C. The resultant was denoted as 3D NiO/NF. The loading weight of NiO was estimated to be approximately 1.6 mg/cm^2 by the weight difference before and after oxidation. For comparison, pristine NiO was synthesized through the chemical deposition approach and followed by sintering at 350 °C.

C. Physical characterization

XRD patterns were recorded using a Rigaku SmartLab X-ray diffractometer (Rigaku Co., Tokyo, Japan) with Cu K_α radiation (λ = 0.15406 nm). Zeiss Sigma FESEM (Zeiss Supra55, Carl Zeiss Group, Oberkochen, Germany) was used to characterize the morphologies. TEM and HRTEM images were taken using Tecnai G2 20 (FEI Company, Eindhoven, Holland). The surface chemical composition and the atomic valence states were investigated by using XPS. XPS was performed under the normal mode by using a Thermo Fisher Scientific Theta Probe Angle-resolved XPS system (Waltham, MA) with monochromatic Al K_α X-ray.

D. Electrochemical characterization

All electrochemical tests were carried out in a three-electrode system using a CHI660B electrochemical station (CH Instruments, Inc., Shanghai, China) in which Ag/AgCl, the Pt wire, and the as-synthesized samples were used as the reference electrode, the counter electrode, and the working electrode, respectively. Commercial Pt/C (20 wt% Pt/XC-72) and NiO powder were loaded on a pretreated NF with a loading of 1.6 mg/cm^2 via drop casting of catalyst ink, respectively. The catalyst ink was a 1 mL solution consisting of 5 mg of catalyst powder, 20 μL of Nafion (5 wt%), 180 μL of ethanol, and 800 μL of DI water. Electrochemical experiments were performed in 1 M KOH electrolyte solution at room temperature. Linear sweep voltammetry (LSV) was used at a scan rate of 5 mV/s to assess the HER performance of the as-synthesized samples. Impedance measurements were carried out over the frequency range from 0.01 Hz to 100 kHz with an amplitude potential of 5 mV. The polarization curves were *iR*-corrected according to ohmic drops obtained from the Nyquist plots. The reference electrode was calibrated with respect to reversible hydrogen electrode (RHE). The calibration was performed in a high purity hydrogen saturated 1 M KOH electrolyte solution with a Pt wire as the working electrode. The chronoamperometry curve was recorded at an overpotential of 70 mV versus RHE, and the chronopotentiometry curve was recorded at a current density of 10 mA/cm^2. The durability of the *i*–*t* curve and the *v*–*t* curve was set to 25 h. Turnover frequency (TOF) was evaluated by the cyclic voltammetry (CV) test in the electrolyte of phosphate buffered solution (pH = 7.0) at a scan rate of 50 mV/s in the potential range from −0.6 to 0.6 V versus Ag/AgCl. The double layer capacitance (C_{dl}) was measured using a simple CV method. The voltage window of cyclic voltammograms was −0.05 to 0.05 V versus Ag/AgCl. The scan rates were 20, 40, 60, 80, 100, 120, 140, 160, 180, and 200 mV/s, respectively. C_{dl} was estimated by plotting $\Delta j = (j_a - j_c)$ at 0.0 V versus Ag/AgCl against the scan rate, where the slope was twice as C_{dl}.

III. RESULTS AND DISCUSSION

Fig. S1 presents the scanning electron microscope (SEM) image of the naked NF. Bare NF displays a smooth surface which provides a rather large area for the deposition of NiO nanoclusters. As can be seen in Fig. 1(a), the surface of the oxidized NF is fully covered by in situ grown NiO nanoclusters. From the magnified image [Fig. 1(b)], the NiO nanoclusters are composed of numerous nanosheets and the sizes of them are in the range from 200 to 300 nm. These NiO nanosheets are interconnected to form a uniform cauliflower-like structure. It is notable that the dark material is bonded tightly to the substrate; even ultrasonication cannot peel off the newly synthesized NiO nanoclusters. The robust combination of NiO and Ni substrate provides a 3D composite with remarkable durability. These cauliflower-like nanostructures with wrinkled surfaces consist of NiO nanoflakes, which have large surface areas that facilitate electron transportation.[39] Furthermore, it is conspicuous that the thin film coated on the NF is cut into many blocks by "slots" with a width of about 30–50 nm. As is reported previously, such unique 3D NiO/Ni heterostructural interfaces play a key role in expediting HER by adsorbing H atoms on Ni sites and releasing the generated OH^- on NiO sites.[26–28] Hence, this unique bifunctional heterostructure endowed the 3D NiO/NF composite with synergistic HER catalytic activity.[27] These "slots" from the as-prepared 3D NiO/NF composite not only act as sinks to store the electrolyte but also lead electrolytes to freely flow inside and outside the structure. In addition, the "slots" structure can provide adequate channels for the resultant hydrogen molecule liberation. More importantly, this structure can expose most of the heterostructurally bifunctional interfaces of NiO/NF, which are beneficial to lowering the kinetic energy barrier of the initial water-dissociation step and promoting the Volmer reaction.[39] As seen from Fig. 1(c), the TEM image shows that the NiO nanosheets are composed of many small near-spherical nanoparticles with a diameter of approximately 8–20 nm. The HRTEM image is displayed in Fig. 1(d). The HRTEM image demonstrates that the majority of the surface is amorphous, implying a high defect concentration of the nanosheets.[40] In addition, the oxygen deficiencies existing on the surface of the NiO crystal can afford numerous active centers to efficiently adsorb and cleave water molecules.[29]

https://doi.org/10.1557/jmr.2017.446 Published online by Cambridge University Press

Fig. 2(a) shows the dark field image of the 3D NiO/NF composite. From Fig. 2(a), the thickness of NiO films is about 500 nm. The elemental distribution mappings of the 3D NiO/NF composite are displayed in Figs. 2(b) and 2(c), confirming the homogeneous distribution of Ni and O on the surface of the 3D NiO/NF composite. EDX (Energy-dispersive X-ray spectroscopy) characterization of the 3D NiO/NF composite is presented in Fig. 2(d). The pattern also shows the presence of Ni and O elements.

To further acquire the structural information of the samples, XRD measurements were carried out. The XRD pattern of pristine NiO is displayed in Fig. S2, and all peaks corresponded well to the Joint Committee on Powder Diffraction Standards card number (JCPDS 71-1179). As shown in Fig. 3(a), the XRD peaks of the 3D NiO/NF composite located at $2\theta = 37.2$, 43.3, and 62.9° are indexed to the (111), (200), and (220) planes of NiO (JCPDS 71-1179), respectively. The diffraction peaks at 44.5, 51.8, and 76.4° are assigned to the (111), (200), and (220) planes of cubic phase nickel (JCPDS 04-0850). All diffraction peaks of the sample match well with the standard card and no impurity peaks are observed, indicating that the as-synthesized sample only contained NiO and Ni. Noticeably, the diffraction peaks of NiO are much weaker compared to the diffraction peaks of Ni [see from Fig. 3(a)], further confirming that the amorphous nanostructure was obtained in the sample. This is consistent with the observation of the HRTEM image.

XPS is an effective technique to analyze surface chemical states. The chemical and surface states of the Ni and O elements of the as-prepared 3D NiO/NF composite were investigated by XPS. The XPS survey spectrum of the 3D NiO/NF composite is shown in Fig. 3(b). The spectrum has been calibrated with the C 1*s* peak to 284.6 eV. Fig. 3(b) reveals the presence of Ni 2*p* and O 1*s* states. Since XPS can only detect the chemical information of a few atomic layers near the surface, the characteristic signal of Ni^0 2*p* at ~852.3 eV is not observed, suggesting that the surfaces of the NF substrate are fully covered by resulting NiO nanoclusters.[26] The observation is consistent with the plots of SEM. The high-resolution XPS spectrum of Ni 2*p* reveals four peaks [Fig. 3(c)]. The main peak of Ni^{2+} at 854.6 eV shifts ~1.5 eV toward higher binding energies; thus, an extremely intense shoulder peak at 856.1 eV is observed. Such a significantly enhanced shoulder peak can mainly be attributed to the effect of defects and surface effects based on the amorphous structure and the large specific surface area of the as-prepared NiO nanoclusters.[41] These

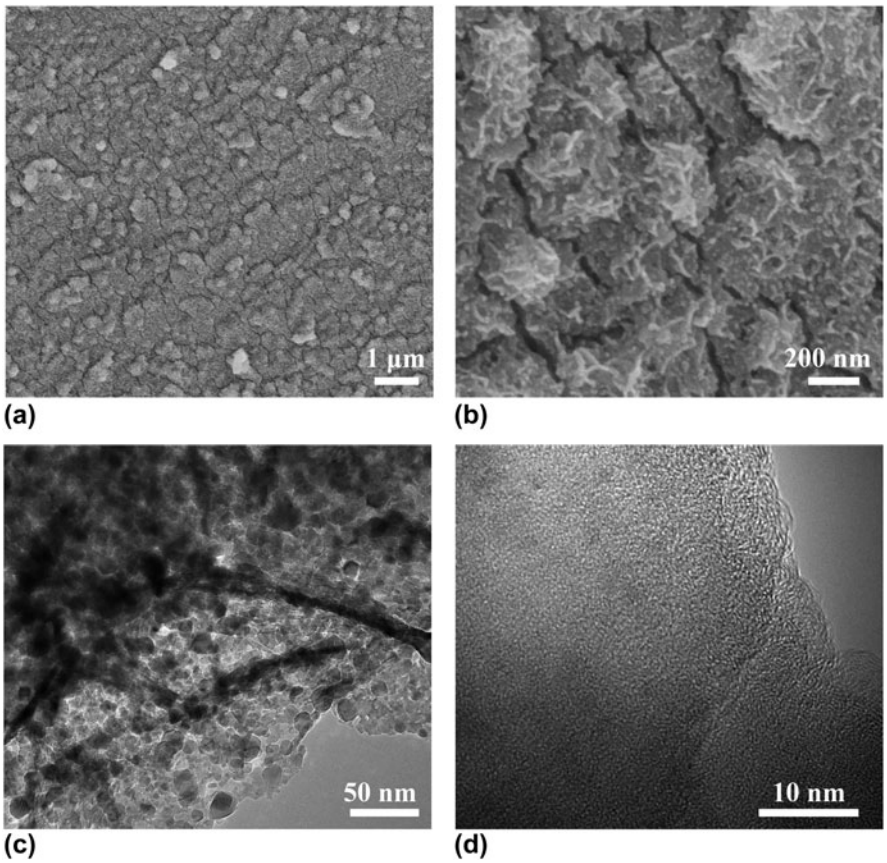


FIG. 1. SEM images of 3D NiO/NF (a) and (b), TEM image of 3D NiO/NF (c), and HRTEM image of 3D NiO/NF (d).

https://doi.org/10.1557/jmr.2017.446 Published online by Cambridge University Press

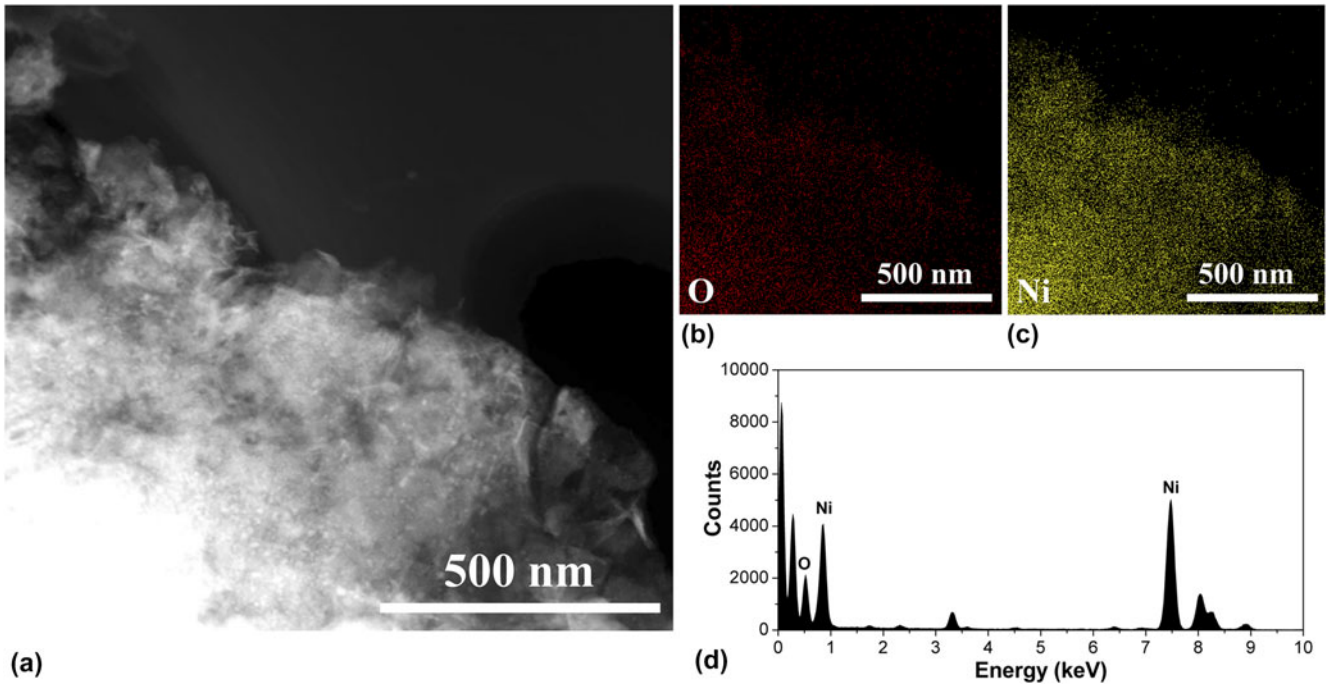


FIG. 2. Dark field image of 3D NiO/NF (a), elemental mapping of O (b) and Ni (c), and EDX spectrum of 3D NiO/NF (d).

results demonstrate that the oxygen-defective structure can be formed in NiO surfaces during the process of reaction, which is responsible for the enhanced electrocatalytic properties of the nanoclusters. Similarly, the high-resolution XPS spectrum of O 1*s* was deconvoluted into three peaks [Fig. 3(d)]. A stronger shoulder peak at 531.5 eV is attributed to the oxygen vacancies of NiO surfaces, indicating that large amounts of oxygen-contained species like H_2O or OH groups are adsorbed. As a result, a high concentration of coordinatively

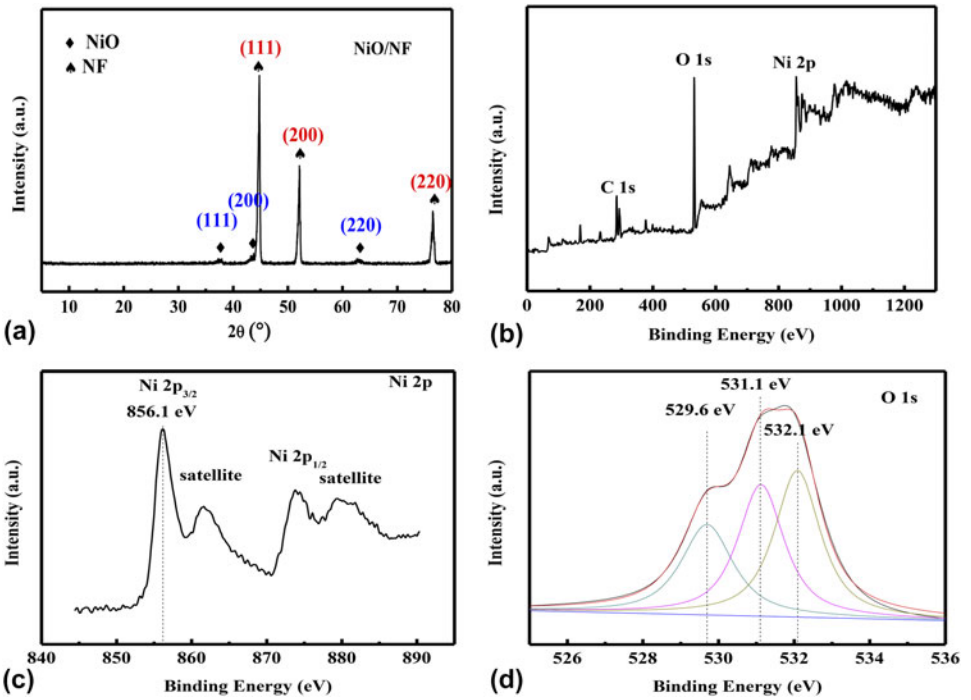


FIG. 3. XRD pattern of 3D NiO/NF (a), XPS survey spectrum of 3D NiO/NF (b), and high-resolution Ni 2*p* (c) and O 1*s* (d) spectra of 3D NiO/NF.

https://doi.org/10.1557/jmr.2017.446 Published online by Cambridge University Press

unsaturated defects at NiO nanocluster surfaces can be further confirmed. These adsorbed hydroxyl groups make the electrode surface more hydrophilic, facilitating the electrolyte to infiltrate into the "slots" of the electrode. Thus, it is rational to conclude that the surfaces of the 3D NiO/NiF composite are dominated by oxygen-defective NiO species. This result is also consistent well with the amorphous feature seen from XRD and HRTEM. As we all know, the smaller size and larger surface area of amorphous nanoparticles are important to provide a large electro-active area for the electrochemical reaction. According to the above-mentioned structure information, the superior performance for electrocatalytical HER of the 3D NiO/NF composite can be expected.

The catalytic performance of the 3D NiO/NF composite was investigated in 1.0 M KOH solution using a standard three-electrode configuration. For comparison, bare NF, pure NiO, and commercial Pt/C were also tested under the same conditions. Potentials were reported versus the RHE according to the formula $E(\mathrm{RHE}) = E(\mathrm{Ag/AgCl}) + 1.026$ V. The polarization curves for the HER of these different four electrodes are recorded in Fig. 4(a). It is obvious that the 3D NiO/NF composite exhibits a remarkable high activity with an onset potential of ~0 V versus RHE and reaches a benchmark HER current density of 10 mA/cm^2 at an overpotential of 70 mV versus RHE. In sharp contrast to the 3D NiO/NF composite, the bare NF and NiO both display inferior catalytic activity with an overpotential of 243 mV and 240 mV at 10 mA/cm^2, respectively. Based on the onset potential, it is obvious that the electrocatalytic activity of the 3D NiO/NF composite is comparable to the commercial Pt/C catalyst. As for the overpotential (at 10 mA/cm^2), the as-prepared 3D NiO/NF composite is also much lower than that of the reported Ni hydroxide-based or Ni oxide-based material (see Table I), such as crystalline/amorphous Ni/NiO core/shell nanosheets,[28] NiO nanoarrays grown on NF,[42] NiO/Ni-CNT heterostructures,[27] NiO_x@BCNTs containing Ni^0 on the interface of Ni/NiO,[26] NiFe layered double hydroxides,[43] and Ni/NiO arrays.[34]

The Tafel plots corresponding to the polarization curves are displayed in Fig. 4(b). The linear regions of the Tafel plots are fitted into the Tafel equation ($\eta = a + b\log(j)$, where b is the Tafel slope), yielding 33, 65, 149, and 189 mV/dec for commercial Pt/C, 3D NiO/NF composite, NiO, and NF electrode, respectively. These results indicate that the 3D NiO/NF composite electrode has a much higher electrocatalytic activity than the naked NF and pristine NiO electrode. Comparing with the Tafel slopes of other previously reported NiO-based catalysts (see Table I), the 3D NiO/NF composite with a lower Tafel slope further demonstrates its superior activity. Though the activity of the 3D NiO/NF composite is still lower than that of the Pt/C electrode, considering that the HER activity in strong base is usually two to three orders lower than in acidic solution, the performance of this electrode is remarkable.

To gain insight into the reaction mechanism of the electrode interface, EIS measurements were completed for the 3D NiO/NF composite and NF sample at $\eta = 150$ mV versus RHE, respectively. The corresponding Nyquist plots are displayed in Fig. 4(c). The Nyquist plots reveal that the series resistances (R_s) of the 3D NiO/NF composite and NF are 1.25 Ω and 1.56 Ω, respectively, which corresponds to a rapid electron transfer through the interface between the electrocatalyst and electrolyte.[44] The high-frequency semicircle is related to the charge transfer resistance (R_{ct}). As for the 3D NiO/NF composite, the suppressed semicircle can be observed, indicating that the charge transfer resistance is ~2.4 Ω, which is much smaller than that of NF (~34 Ω). It can be inferred that smaller R_{ct} is a major contributor for the kinetics at the 3D NiO/Ni interface in our system.

It is well known that the pathway of the HER in alkaline media involves two principal steps, that is, the Volmer–Heyrovsky process or Volmer–Tafel process: the Volmer step, where water dissociation and formation of an active intermediate H_{ads} ($H_2O + e^- \rightarrow H_{ads} + OH^-$), followed by either the Heyrovsky step ($H_2O + H_{ads} + e^- \rightarrow H_2 + OH^-$) or the Tafel step ($H_{ads} + H_{ads} \rightarrow H_2$).[26–28] In detail, these two processes involve the adsorption of H_2O molecule, the Volmer reduction of adsorbed H_2O into adsorbed OH^- and H_{ads} intermediate, desorption of OH^- to leave the surface, and recombination of H_{ads} intermediates for H_2 evolution. As displayed in Fig. 4(a), a pure NiO surface is inactive for HER due to the lack of H adsorption sites, whereas, on a pure NF surface, the strong adsorption of the formed OH^- species can occupy the sites for H atom, which is responsible for the sluggish HER kinetics.[45] Therefore, water dissociation on the pure Ni surface and H_{ads} absorption on the NiO surface are all kinetically difficult. Hereby, we can rationally conjecture that the water dissociation and desorption of formed H_2 gas in alkaline media can happen in NiO and Ni sites, respectively.[26] On a NiO/Ni interface, the OH^- produced by H_2O decomposition can preferentially adhere to a NiO site at the interface due to a high concentration of coordinatively unsaturated defects, while a neighboring Ni site facilitates H adsorption where two atomic H_{ads} intermediates on the Ni surface recombine to form H_2, i.e., a Tafel step occurs.[26,27] Finally, the resultant H_2 and OH^- desorb from the Ni domain and NiO domain, respectively, followed by adsorption of another water molecule at the same site (see Scheme 1). In general, the Tafel slope is an indicator of the rate-determining step (RDS) in the HER mechanism. The Tafel slope of 120, 40, or 30 mV/dec is expected if the Volmer, Heyrovsky, or Tafel step is the RDS, respectively. However, a slope of ~65 mV/dec

https://doi.org/10.1557/jmr.2017.446 Published online by Cambridge University Press

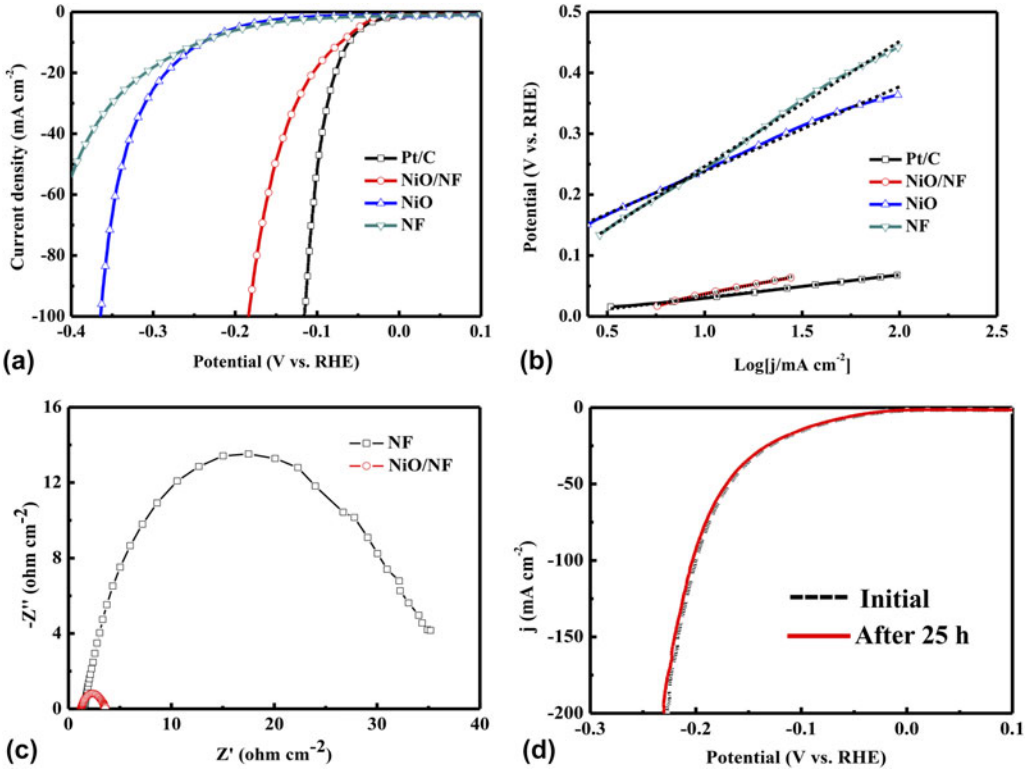


FIG. 4. Electrochemical measurements of various materials in 1 M KOH aqueous solution: (a) polarization curves, (b) Tafel plots (the black dashed lines are the linear fitting results of corresponding Tafel curves), (c) Nyquist plots of the bare NF and NiO/NF composite electrodes, and (d) polarization curves (5 mV/s) comparison of 3D NiO/NF between the initial state and the chronoamperometry measurement after 25 h.

observed here for the 3D NiO/NF composite lies between the characteristic slopes of 40 and 120 mV/dec, indicating that neither the Heyrovsky nor the Volmer step is the RDS. For HER, a Tafel slope near 60 mV/dec has been ascribed to possible hydrogen spillover effects (surface chemical rearrangements).[45] For the 3D NiO/NF composite, H_{ads} intermediates moving from NiO sites to nearby metallic Ni sites can be relatively difficult (two short arrows seen from Scheme 1); thus surface chemical rearrangement of atomic H is rate-determining.[46] The spillover path is mainly determined by the length of the NiO and Ni interface edges, and thus more exposed active interfaces are even more important than the loading and morphology of the catalyst.[47] In the present work, since unique "slots" morphologies can significantly increase the interface edge length, the RDS is hugely accelerated, which accounts for its extremely low overpotential and small Tafel slope of the 3D NiO/NF composite. Based on the above analysis, the superior HER activity of the 3D NiO/NF composite electrode can be attributed to the following reasons: (i) The coordinatively unsaturated defects at the NiO surface can facilitate the disassociation of adsorbed water. (ii) Unique "slots" morphology of the as-prepared 3D NiO/NF cannot only expose most bifunctional and heterostructural interfaces, which is beneficial to reducing the kinetic energy barrier of the initial water dissociation step, but also benefit mass transport and H_2 evolution. Importantly, the unique "slots" morphology can also offer a large interface edge length and more spillover paths which facilitate surface chemical rearrangements of atomic H_{ads} intermediates, accelerating the RDS. (iii) The conductive network structure of the metal Ni substrate also further improves the electric conductivity of the electrode, benefitting the charge transfer. The synergistic effect at the NiO/NF interface is perfectly realized.

TABLE I. Comparison of the performance of $Ni(OH)_2$- and NiO-based HER catalysts in alkaline media (1 M KOH or NaOH).

Catalyst	Current density (j, mA/cm^2)	η at the corresponding j (mV)	Tafel slope (mV/dec)	Ref.
NiO_x@BCNTs	10	79	96	26
NiO/Ni-CNT	10	<100	82	27
Ni/NiO core/shell nanosheets	10	145	43	28
Ni/NiO array	20	46	65	29
NiO nanoarrays grown on NF	10	310	222	42
NiFe layered double hydroxide	10	210	...	43
NiO/NF	10	70	65	This work

https://doi.org/10.1557/jmr.2017.446 Published online by Cambridge University Press

Electrocatalytic stability is another important criterion for the HER catalysts. The long-term electrochemical stability tests for the 3D NiO/NF composite were continuously carried out in 1.0 M KOH solution. The chronoamperometry measurement was conducted at a preset potential of 70 mV versus RHE for 25 h. The *i–t* curve of the 3D NiO/NF composite is shown in Fig. S3(a). The current density was still kept constant after 25 h for HER, demonstrating the excellent durability and high activity of the 3D NiO/NF composite over long-time testing. Similarly, the chronopotentiometry measurement was also conducted at a preset current density of 10 mA/cm^2 for 25 h, and the *v–t* curve of the 3D NiO/NF composite is displayed in Fig. S3(b). In addition, after 25 h of the chronoamperometry test, the LSV plot was collected again. As shown in Fig. 4(d), the LSV curves of the 3D NiO/NF composite electrode before and after 25 h of electrolysis nearly overlapped with each other. When reaching a current density of 10 mA/cm^2 again, the required overpotential negligibly increased, further confirming its noticeable electrochemical stability. Such excellent long-term stability is attributed to the robustness of the electrode which originates from the tight connection between the amorphous NiO and the NF substrate by the in situ oxidation fabrication approach.

Taking account of a large NiO/Ni interface is likely critical to achieve a high catalytic activity, the surface effects of the 3D NiO/NF composite catalyst were also studied. Obtaining the exact surface area is difficult due to the unknown capacitive behavior of the electrode. However, the electrochemically active surface area (ECSA) of the catalysts can be estimated from C_{dl}, as C_{dl} is linearly proportional to the effective active surface area.[46] The linear slope of the capacitive current against the scan rate is used to represent the ECSA.[48,49] Typical cyclic voltammograms of the 3D NiO/NF composite and NF with various scan rates (20–200 mV/s) in the region of −0.05–0.05 V versus Ag/AgCl in 1.0 M KOH solution are shown in Figs. 5(a) and S4, respectively. All curves display regular rectangle which means that the current response in this region is attributed to the charging of the double layer.[49,50] Fig. 5(b) shows the fitting curves of the measured current density differences at 0.0 V versus Ag/AgCl as a function with scan rate. Remarkably, the 3D NiO/NF composite electrode yields a high capacitance

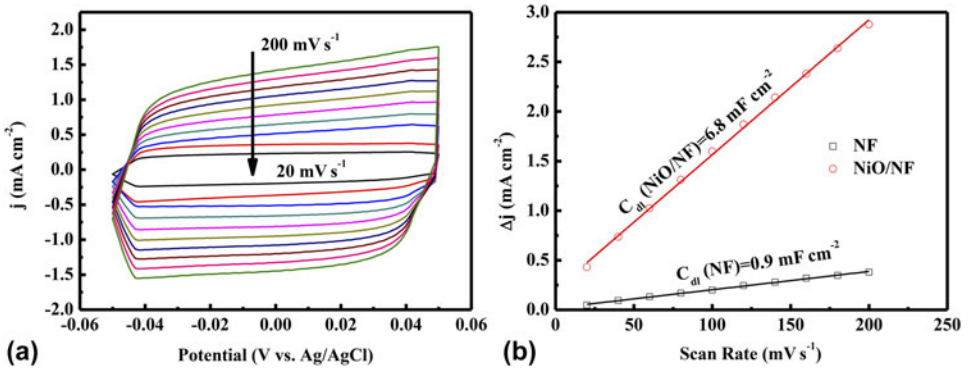


FIG. 5. Cyclic voltammograms of the 3D NiO/NF recorded at pH = 14 and between −0.05 V and +0.05 V versus Ag/AgCl at a scan rate of 50 mV/s (a) and the charging current density differences ($\Delta j = j_a - j_c$) plotted against scan rate (b).

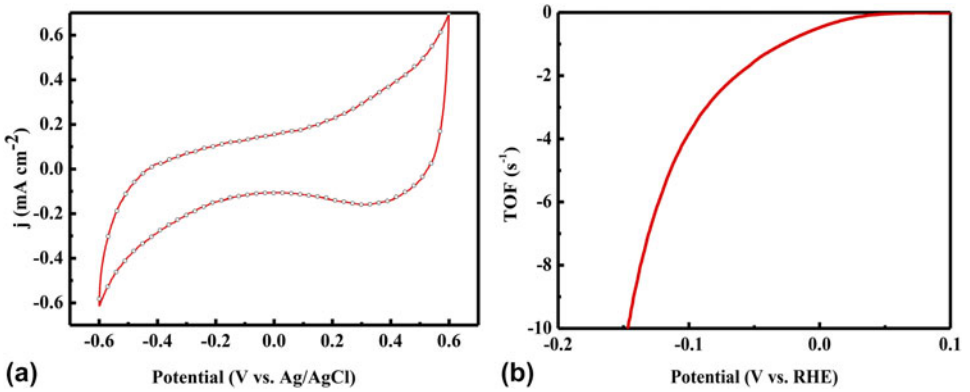


FIG. 6. CV curve of the 3D NiO/NF collected in phosphate buffered solution (pH = 7) at a scan rate of 50 mV/s in the potential range from −0.6 to 0.6 V versus Ag/AgCl (a) and plot of the calculated TOFs for the 3D NiO/NF composite against overpotential at pH = 14 (b).

https://doi.org/10.1557/jmr.2017.446 Published online by Cambridge University Press

value up to 6.8 mF/cm^2, substantially larger than the NF (0.9 mF/cm^2) electrodes. Moreover, the roughness factor (RF) can be calculated from the ratio of the ECSA to the real surface area of the electrode. Hence, it is estimated to be about 340 for the 3D NiO/NF composite and 45 for the NF, respectively. Clearly, the 3D NiO/NF composite possesses seven times larger active surface area than the NF, indicating that the large surface area and more exposed active sites in the 3D NiO/NF interfaces were created by a facile in situ oxidation, consistent with the observation of SEM.

The TOF is an important parameter to reflect the intrinsic catalytic activity of the electrocatalysts, and the estimation of TOFs makes it possible to compare the activity with diverse catalysts.[40] To gain further insight into the intrinsic catalytic activity of the as-prepared 3D NiO/NF composite electrode, the TOF values of the above catalysts were calculated based on a common method reported in previous studies.[40] Fig. 6(a) shows the cyclic voltammograms in the region from −0.6 to 0.6 V versus Ag/AgCl for the 3D NiO/NF composite at a scan rate of 50 mV/s in phosphate buffered solution (pH = 7). The integrated charge over the whole potential range may be proportional to the total number of active sites.[40] Assuming a one-electron process for both reduction and oxidation, the upper limit of the active sites (n) can be calculated by the equation $n = Q/2F$, where Q is the number of voltammetric charges and F is Faraday constant. The calculated Q and n values for the 3D NiO/NF composite electrode are 8.14 mF/cm^2 and 2.54×10^{16} cm^{-2}, respectively. This, thus, confirms the increased active sites for the 3D NiO/NF composite. In addition, the TOFs can be calculated according to the equation TOF = $I/2Fn$, where I is the current during the LSV measurement. Fig. 6(b) shows the polarization curve of the 3D NiO/NF composite at pH = 14, normalized by the number of active sites and expressed in terms of TOF. The most active catalyst, Pt, has a TOF of 0.8 s^{-1} at $\eta = 0$, whereas the as-prepared 3D NiO/NF composite reaches a TOF of 0.6 s^{-1} at $\eta = 0$, implying the superior intrinsic catalytic activity of the NiO/NF composite for HER, which is consistent with the results obtained from LSV measurements. Thus, the as-synthesized 3D NiO/NF composite may hold a promising future in hydrogen generation through the electrochemical water splitting.

IV. CONCLUSIONS

In summary, the 3D NiO/NF composite can be synthesized using a facile low-temperature-oxidation method. When this 3D NiO/NF composite was used as the electrocatalyst for HER in the alkaline media, it exhibited a top-level HER performance including a low overpotential (70 mV) at a current density of 10 mA/cm^2, an exceptional Tafel slope (65 mV/dec), and excellent HER stability. The unique "slots" morphology of the composite cannot only offer large interface edge length and more spillover paths but also facilitate electrolyte permeation into exposed active interfaces. The coordinatively unsaturated defects at the amorphous NiO surfaces can accelerate disassociation of adsorbed water, promoting the initial Volmer reaction, and the metallic Ni substrate can enhance the conductivity and facilitate H adsorption. The kinetic energy barrier of water dissociation can be effectively reduced because of the synergetic effect of metallic Ni and amorphous NiO. The rough surface and extremely large TOF also contributed substantially to the high activity for HER. Our findings show that the 3D NiO/NF composite can be a highly promising electrocatalyst for electrochemical hydrogen generation. Meanwhile, this study may provide a new methodology for designing metal oxides/metal catalysts for electrolysis of water.

ACKNOWLEDGMENTS

This work was supported by the National Natural Science Foundation of China (Grant No. 51372080) and the Research Foundation of Education Bureau of Hunan Province, China (Grant Nos. 16C0717 and 17K039).

REFERENCES

1. J.A. Turner: Sustainable hydrogen production. *Science* **305**, 972 (2004).
2. G.S. Hutchings, Y. Zhang, J. Li, B.T. Yonemoto, X. Zhou, K. Zhu, and F. Jiao: In situ formation of cobalt oxide nanocubanes as efficient oxygen evolution catalysts. *J. Am. Chem. Soc.* **137**, 4223 (2015).
3. X.X. Zou and Y. Zhang: Noble metal-free hydrogen evolution catalysts for water splitting. *Chem. Soc. Rev.* **44**, 5148 (2015).
4. B. Hinnemann, P.G. Moses, J. Bonde, K.P. Jørgensen, J.H. Nielsen, S. Horch, I. Chorkendorff, and J.K. Nørskov: Biomimetic hydrogen evolution: MoS_2 nanoparticles as catalyst for hydrogen evolution. *J. Am. Chem. Soc.* **127**, 5308 (2005).
5. J.K. Norskov and C.H. Christensen: Toward efficient hydrogen production at surfaces. *Science* **312**, 1322 (2006).
6. T.F. Jaramillo, K.P. Jørgensen, J. Bonde, J.H. Nielse, and S. Horch: Identification of active edge sites for electrochemical H_2 evolution from MoS_2 nanocatalysts. *Science* **317**, 100 (2007).
7. M.A. Lukowski, A.S. Daniel, F. Meng, A. Forticaux, L.S. Li, and S. Jin: Enhanced hydrogen evolution catalysis from chemically exfoliated metallic MoS_2 nanosheets. *J. Am. Chem. Soc.* **135**, 10274 (2013).
8. Y. Zhang, Y. Xie, Y. Zhou, X. Wang, and K. Pan: Well dispersed Fe_2N nanoparticles on surface of nitrogen-doped reduced graphite oxide for highly efficient electrochemical hydrogen evolution. *J. Mater. Res.* **32**, 1770 (2017).
9. S.C. Lin, Y.F. Chiu, P.W. Wu, Y.F. Hsieh, and C.Y. Wu: Templated fabrication of nanostructured Ni brush for hydrogen evolution reaction. *J. Mater. Res.* **25**, 2001 (2011).
10. I.S. McKay, J.A. Schwalbe, E.D. Goodman, J.J. Willis, A. Majumdar, and M. Cargnello: Elucidating the synergistic

https://doi.org/10.1557/jmr.2017.446 Published online by Cambridge University Press

mechanism of nickel–molybdenum electrocatalysts for the hydrogen evolution reaction. *MRS Commun.* **6**, 241 (2016).
11. M. Blouin, D. Guay, J. Huot, and R. Schulz: High energy ball-milled Ti_2RuFe electrocatalyst for hydrogen evolution in the chlorate industry. *J. Mater. Res.* **12**, 1492 (1997).
12. L. Tian, J.B. Murowchick, and X. Chen: Improving the activity of Co_xP nanoparticles for electrochemical hydrogen evolution by hydrogenation. *Sustainable Energy Fuels* **1**, 62 (2017).
13. L. Tian, X. Yan, X. Chen, L. Liu, and X. Chen: One-pot, large-scale, facile synthesis of Co_xP nanocatalysts for electrochemical hydrogen evolution. *J. Mater. Chem. A* **4**, 13011 (2016).
14. L. Tian, X. Yan, and X. Chen: Electrochemical activity of iron phosphide nanoparticles in hydrogen evolution reaction. *ACS Catal.* **6**, 5441 (2016).
15. J.R. McKone, B.F. Sadtler, C.A. Werlang, N.S. Lewis, and H.B. Gray: Ni–Mo nanopowders for efficient electrochemical hydrogen evolution. *ACS Catal.* **3**, 166 (2013).
16. C. González-Buch, I. Herraiz-Cardona, E. Ortega, J. García-Antón, and V. Pérez-Herranz: Study of the catalytic activity of 3D macroporous Ni and NiMo cathodes for hydrogen production by alkaline water electrolysis. *J. Appl. Electrochem.* **46**, 791 (2016).
17. R. Solmaz and G. Kardas: Electrochemical deposition and characterization of NiFe coatings as electrocatalytic materials for alkaline water electrolysis. *Electrochim. Acta* **54**, 3726 (2009).
18. X. Wang, R. Su, H. Aslan, J. Kibsgaard, S. Wendt, L. Meng, M. Dong, Y. Huang, and F. Besenbacher: Tweaking the composition of NiMoZn alloy electrocatalyst for enhanced hydrogen evolution reaction performance. *Nano Energy* **12**, 9 (2015).
19. C.G. Buch, I.H. Cardona, E. Ortega, J.G. Anton, and V.P. Herranz: Study of the catalytic activity of 3D macroporous Ni and NiMo cathodes for hydrogen production by alkaline water electrolysis. *J. Appl. Electrochem.* **46**, 791 (2016).
20. M.M. Jaksic: Electrocatalysis of hydrogen evolution in the light of the brewer-engel theory for bonding in metals and intermetallic phases. *Electrochim. Acta* **29**, 1539 (1984).
21. L.L. Feng, G.T. Yu, Y.Y. Wu, G.D. Li, H. Li, Y. Sun, T. Asefa, W. Chen, and X. Zou: High-index faceted Ni_3S_2 nanosheet arrays as highly active and ultrastable electrocatalysts for water splitting. *J. Am. Chem. Soc.* **137**, 14023 (2015).
22. G.F. Chen, T.Y. Ma, Z.Q. Liu, N. Li, Y.Z. Su, K. Davey, and S.Z. Qiao: Efficient and stable bifunctional electrocatalysts Ni/Ni_xM_y (M = P, S) for overall water splitting. *Adv. Funct. Mater.* **26**, 3314 (2016).
23. J.L. Lv, H. Miura, Y. Meng, and T.X. Liang: Synthesis of Ni_3S_2 nanotube arrays on nickel foam by catalysis of thermal reduced graphene for hydrogen evolution reaction. *Appl. Surf. Sci.* **399**, 769 (2017).
24. J.Y. Li, J. Li, X.M. Zhou, Z.M. Xia, W. Gao, Y.Y. Ma, and Y.Q. Qu: Highly efficient and robust nickel phosphides as bifunctional electrocatalysts for overall water-splitting. *ACS Appl. Mater. Interfaces* **8**, 10826 (2016).
25. Y.F. Xu, M.R. Gao, Y.R. Zheng, J. Jiang, and S.H. Yu: Nickel/nickel(II) oxide nanoparticles anchored onto cobalt(IV) diselenide nanobelts for the electrochemical production of hydrogen. *Angew. Chem., Int. Ed.* **52**, 8546 (2013).
26. J. Wang, S. Mao, Z. Liu, Z. Wei, H. Wang, Y. Chen, and Y. Wang: Dominating role of Ni^0 on the interface of Ni/NiO for enhanced hydrogen evolution reaction. *ACS Appl. Mater. Interfaces* **9**, 7139 (2017).
27. M. Gong, W. Zhou, M.C. Tsai, J. Zhou, M. Guan, M.C. Lin, B. Zhang, Y. Hu, D.Y. Wang, J. Yang, S.J. Pennycook, B.J. Hwang, and H. Dai: Nanoscale nickel oxide/nickel heterostructures for active hydrogen evolution electrocatalysis. *Nat. Commun.* **5**, 4695 (2014).
28. X. Yan, L. Tian, and X. Chen: Crystalline/amorphous Ni/NiO core/shell nanosheets as highly active electrocatalysts for hydrogen evolution reaction. *J. Power Sources* **300**, 336 (2015).
29. X. Yan, L. Tian, K. Li, S. Atkins, H. Zhao, J. Murowchick, L. Liu, and X. Chen: $FeNi_3/NiFeO_x$ nanohybrids as highly efficient bifunctional electrocatalysts for overall water splitting. *Adv. Mater. Interfaces* **3**, 1600368 (2016).
30. X. Yan, L. Tian, S. Atkins, Y. Liu, J. Murowchick, and X. Chen: Converting $CoMoO_4$ into CoO/MoO_x for overall water splitting by hydrogenation. *ACS Sustainable Chem. Eng.* **4**, 3743 (2016).
31. X. Yan, L. Tian, J.B. Murowchick, and X. Chen: Partially amorphized $MnMoO_4$ for highly efficient energy storage and hydrogen evolution reaction. *J. Mater. Chem. A* **4**, 3683 (2016).
32. X. Yan, K. Li, L. Lyu, F. Song, J. He, D. Niu, L. Liu, X. Hu, and X. Chen: From water oxidation to reduction: Transformation from $Ni_xCo_{3-x}O_4$ nanowires to $NiCo/NiCoO_x$ heterostructures. *ACS Appl. Mater. Interfaces* **8**, 3208 (2016).
33. X. Yan, L. Tian, M. He, and X. Chen: Three-dimensional crystalline/amorphous Co/Co_3O_4 core/shell nanosheets as efficient electrocatalysts for the hydrogen evolution reaction. *Nano Lett.* **15**, 6015 (2015).
34. X. Liu, X. Wang, X. Yuan, W. Dong, and F. Huang: Rational composition and structural design of in situ grown nickel-based electrocatalysts for efficient water electrolysis. *J. Mater. Chem. A* **4**, 167 (2016).
35. Z. Zhang, Q. Wang, C. Zhao, S. Min, and X. Qian: One-step hydrothermal synthesis of 3D petal-like $Co_9S_8/RGO/Ni_3S_2$ composite on nickel foam for high-performance supercapacitors. *ACS Appl. Mater. Interfaces* **7**, 4861 (2015).
36. R. Subbaraman, D. Tripkovic, D. Strmcnik, K.C. Chang, M. Uchimura, A.P. Paulikas, V. Stamenkovic, and N.M. Markovic: Enhancing hydrogen evolution activity in water splitting by tailoring Li^+–$Ni(OH)_2$–Pt interfaces. *Science* **334**, 1256 (2011).
37. M.K. Bates, Q. Jia, N. Ramaswamy, R.J. Allen, and S. Mukerjee: Composite $Ni/NiO–Cr_2O_3$ catalyst for alkaline hydrogen evolution reaction. *J. Phys. Chem. C* **119**, 5467 (2015).
38. M.S. Faber and S. Jin: Earth-abundant inorganic electrocatalysts and their nanostructures for energy conversion applications. *Energy Environ. Sci.* **7**, 3519 (2014).
39. Y. Zhang, P. Ju, C. Zhao, and X. Qian: In-situ grown of $MoS_2/RGO/MoS_2$@Mo nanocomposite and its supercapacitor performance. *Electrochim. Acta* **219**, 693 (2016).
40. D. Merki, S. Fierro, H. Vrubel, and X.L. Hu: Amorphous molybdenum sulfide films as catalysts for electrochemical hydrogen production in water. *Chem. Sci.* **2**, 1262 (2011).
41. L. Soriano, I. Preda, A. Gutiérrez, and S. Palacín: Surface effects in the Ni 2*p* X-ray photoemission spectra of NiO. *Phys. Rev. B* **75**, 233417 (2007).
42. J. Zheng, W. Zhou, T. Liu, S. Liu, C. Wang, and L. Guo: Homologous $NiO//Ni_2P$ nanoarrays grown on nickel foams: A well matched electrode pair with high stability in overall water splitting. *Nanoscale* **9**, 4409 (2017).
43. J. Luo, J.H. Im, M.T. Mayer, M. Schreier, M.K. Nazeeruddin, N.G. Park, S.D. Tilley, H.J. Fan, and M. Grätzel: Water photolysis at 12.3% efficiency via perovskite photovoltaics and earth-abundant catalysts. *Science* **345**, 1593 (2014).
44. S.T. Finn and J.E. Macdonald: Contact and support considerations in the hydrogen evolution reaction activity of petaled MoS_2 electrodes. *ACS Appl. Mater. Interfaces* **8**, 25185 (2016).
45. J. Zhang, T. Wang, P. Liu, S. Liu, R. Dong, X. Zhuang, M. Chen, and X. Feng: Engineering water dissociation sites in MoS_2 nanosheets for accelerated electrocatalytic hydrogen production. *Energy Environ. Sci.* **9**, 2789 (2016).

https://doi.org/10.1557/jmr.2017.446 Published online by Cambridge University Press

46. I.M. Kodintsev and S. Trasatti: Electrocatalysis of H_2 evolution on RuO_2 + IrO_2 mixed oxide electrodes. *Electrochim. Acta* **39**, 1803 (1994).
47. I.A. Pašti, M. Leetmaa, and N.V. Skorodumova: General principles for designing supported catalysts for hydrogen evolution reaction based on conceptual Kinetic Monte Carlo modeling. *Int. J. Hydrogen Energy* **41**, 2526 (2016).
48. M.A. Lukowski, A.S. Daniel, C.R. English, F. Meng, A. Forticaux, R.J. Hamers, and S. Jin: Highly active hydrogen evolution catalysis from metallic WS_2 nanosheets. *Energy Environ. Sci.* **7**, 2608 (2014).
49. D. Merki, H. Vrubel, L. Rovelli, S. Fierro, and X. Hu: Fe, Co, and Ni ions promote the catalytic activity of amorphous molybdenum sulfide films for hydrogen evolution. *Chem. Sci.* **3**, 2515 (2012).
50. F. Li, J. Li, X. Lin, X. Li, Y. Fang, L. Jiao, X. An, Y. Fu, J. Jin, and R. Li: Designed synthesis of multi-walled carbon nanotubes@-Cu@MoS_2 hybrid as advanced electrocatalyst for highly efficient hydrogen evolution reaction. *J. Power Sources* **300**, 301 (2015).

Supplementary Material

To view supplementary material for this article, please visit https://doi.org/10.1557/jmr.2017.446.

https://doi.org/10.1557/jmr.2017.446 Published online by Cambridge University Press